Scaffold topography alters intracellular calcium dynamics in cultured cardiomyocyte networks

Lihong Yin,[1],* Harold Bien,[1],* and Emilia Entcheva[1,2]

Departments of [1]Biomedical Engineering and [2]Physiology and Biophysics,
Stony Brook University, Stony Brook, New York 11794

Yin, Lihong, Harold Bien, and Emilia Entcheva. Scaffold topography alters intracellular calcium dynamics in cultured cardiomyocyte networks. *Am J Physiol Heart Circ Physiol* 287: H1276–H1285, 2004. First published April 22, 2004; 10.1152/ajpheart.01120.2003.—Structural and functional changes ensue in cardiac cell networks when cells are guided by three-dimensional scaffold topography. We report enhanced synchronous pacemaking activity in association with slow diastolic rise in intracellular Ca^{2+} concentration ($[Ca^{2+}]_i$) in cell networks grown on microgrooved scaffolds. Topography-driven changes in cardiac electromechanics were characterized by the frequency dependence of $[Ca^{2+}]_i$ in syncytial structures formed of ventricular myocytes cultured on microgrooved elastic scaffolds (G). Cells were electrically paced at 0.5–5 Hz, and $[Ca^{2+}]_i$ was determined using microscale ratiometric (fura 2) fluorescence. Compared with flat (F) controls, the G networks exhibited elevated diastolic $[Ca^{2+}]_i$ at higher frequencies, increased systolic $[Ca^{2+}]_i$ across the entire frequency range, and steeper restitution of Ca^{2+} transient half-width ($n = 15$ and 7 for G and F, respectively, $P < 0.02$). Significant differences in the frequency response of force-related parameters were also found, e.g., overall larger total area under the Ca^{2+} transients and faster adaptation of relaxation time to pacing rate ($P < 0.02$). Altered $[Ca^{2+}]_i$ dynamics were paralleled by higher occurrence of spontaneous Ca^{2+} release and increased sarcoplasmic reticulum load ($P < 0.02$), indirectly assessed by caffeine-triggered release. Electromechanical instabilities, i.e., Ca^{2+} and voltage alternans, were more often observed in G samples. Taken together, these findings *1*) represent some of the first functional electromechanical data for this in vitro system and *2*) demonstrate direct influence of the microstructure on cardiac function and susceptibility to arrhythmias via Ca^{2+}-dependent mechanisms. Overall, our results substantiate the idea of guiding cellular phenotype by cellular microenvironment, e.g., scaffold design in the context of tissue engineering.

frequency; sarcoplasmic reticulum load; cardiac tissue engineering; arrhythmogenesis

A DOMINANT PORTION OF CARDIAC arrhythmias is associated with underlying structural abnormalities (23, 33). Knowledge of how cardiac structure affects function may result in improved prediction and management of arrhythmias. A valid and versatile in vitro model is a prerequisite for better understanding of the structure-function relation. Cardiomyocytes cultured on growth-directed substrates offer a suitable and convenient experimental system for exploring interactions in this regard.

Aligned collagen substrates (17), microabraded coverslips (8), and micropatterned lines (8, 28) have been used to enforce cell surface attachment restrictions and to exert geometric control of cultured cardiomyocytes. The resultant altered morphology and connectivity have been linked to cellular reprogramming, including changes in ion channels (35) and in conduction patterns at the multicellular level (8, 17). Although such geometric confinements demonstrate the power of affecting function through structure, recently concerns have been raised about the relevance of this traditional two-dimensional cell culture setting to the in vivo three-dimensional cellular microenvironment (20). Matrix topography, molecular composition, and pliability are strong effectors of the mode of cellular attachment, cytoskeletal architecture, and overall function of culture-grown cells. A higher level of sophistication in designing in vitro model systems for basic cardiovascular studies can be achieved by the use of textured surfaces to create a rudimentary three-dimensional microenvironment with out-of-plane attachment options. Topographic influences on cell structure have been reported for noncardiac (10, 30) and cardiac cells (14), including cellular alignment and cytoskeletal rearrangement (12). The corresponding functional changes incurred in cardiomyocytes as a result of three-dimensional cell guidance are particularly valuable in understanding basic material-cell interactions for tissue engineering applications and in dissecting proarrhythmic consequences of structural heart disease. Such functional changes are yet to be characterized in depth.

Our group has adopted the experimental approach of designing syncytial cardiac networks in simplified three-dimensional cell microenvironments by the use of deeply (20–50 µm) microgrooved surfaces. We previously reported structural changes in such networks, including enhanced actin cytoskeleton organization, improved intragroove cellular gap junctional connectivity (6), and higher nuclear eccentricity (15). These structural changes were also accompanied by an apparent increase in frequency of synchronized spontaneous activity and higher uniaxial cellular strains developed on microgrooved than on control flat surfaces (6).

In the present study, we ask the following questions: *1*) Does cell rearrangement, guided by surface texture, lead to altered intracellular Ca^{2+} dynamics? *2*) What is the extent of these changes? We hypothesized that alterations in intracellular Ca^{2+} handling will follow the cytoskeletal and overall morphological changes induced in our simplified three-dimensional setting, as suggested in previous studies (25). Furthermore, we hypothesized that such alterations might provide the substrate for increased pacemaking activity and, possibly, include proarrhythmic features that could be used as a model of

---

* L. Yin and H. Bien contributed equally to this work.

Address for reprint requests and other correspondence: E. Entcheva, Dept. Biomedical Engineering, Stony Brook Univ., HSC T18-030, Stony Brook, NY 11794-8181 (E-mail: emilia.entcheva@sunysb.edu).
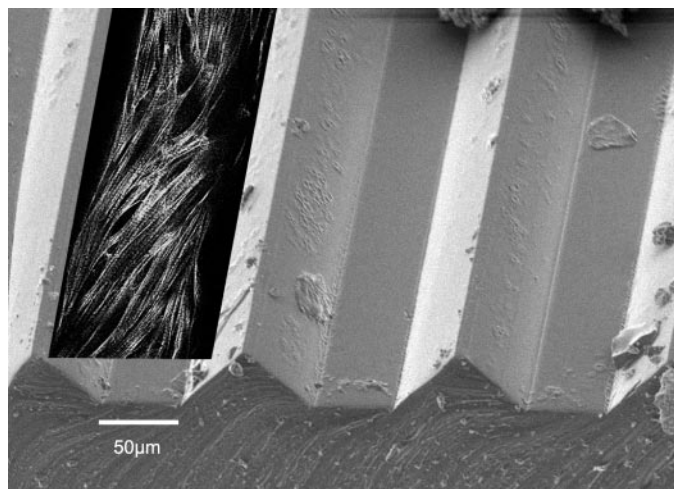
Fig. 1. Scaffold topography: a collage of an actual scanning electron microscopy image of a microfabricated scaffold combined with a single confocal section of fluorescently labeled actin cytoskeleton of cells grown on the microgrooved surface. Surface included deep trapezoidal grooves with a depth of 50 μm and 120-μm spacing between adjacent triangular ridges. Cells grown on microgrooved surfaces exhibited well-organized sarcomered actin (as shown through fluorescent labeling) and had a preferential orientation (anisotropy).

cardiac arrhythmias. Ca^{2+} transients, obtained in ratiometric fura 2 experiments, were evaluated at frequencies of 0.5–5 Hz. Our results constitute the first systematic characterization of frequency-dependent intracellular Ca^{2+} concentration ([Ca^{2+}]$_i$) handling in a multicellular cultured cardiomyocyte model system, in a simple two-dimensional (monolayer) setting, and on introduction of three-dimensional topography. We show that a defined change in scaffold topography can lead to a series of Ca^{2+}-handling modifications, including increased rate of diastolic Ca^{2+} rise, elevated diastolic and systolic Ca^{2+} levels, and steeper restitution of Ca^{2+} transient duration. Combined with observations for increased occurrence of spontaneous Ca^{2+} release and Ca^{2+} instabilities (alternans) on grooved surfaces, our data suggest topography-altered force development and altered propensity to arrhythmias.

MATERIALS AND METHODS

Isolation and culture of neonatal ventricular myocytes. The ventricles of the hearts of 3-day-old Sprague-Dawley rats were minced into small fragments and placed in Hanks' balanced salt solution (GIBCO Invitrogen, Carlsbad, CA). Enzymatic digestion was applied using trypsin (1 mg/ml, 4°C overnight; US Biochemicals, Cleveland, OH) and then collagenase (1 mg/ml, 37°C; Worthington Biomedical, Lakewood, NJ). After centrifugation, the supernatant was discarded and the cells were resuspended in culture medium consisting of medium 199 (GIBCO), 12 μM L-glutamine (GIBCO), 0.05 μg/ml penicillin-streptomycin (Mediatech Cellgro, Kansas City, MO), 0.2 μg/ml vitamin B$_{12}$ (Sigma, St. Louis, MO), 10 mM HEPES (GIBCO), and 3.5 mg/ml D-(+)-glucose (Sigma) supplemented with 10% fetal bovine serum (GIBCO). Two-step preplating for a total of 90 min was used to eliminate fibroblasts from the cell population. The cardiomyocytes were then seeded on fibronectin-coated surfaces (50 μg/ml; BD Biosciences, Franklin Lakes, NJ) at a high density (0.4 × 10^6 cells/cm^2) and kept at 37°C in 5% CO$_2$ in culture medium with 10% serum on *days 1* and *2* and then switched to culture medium with 2% serum changed every other day. Cells formed syncytial structures, confirmed by macroscopic mapping of electrical propagation (6).

Scaffold manufacture. Scaffolds for cell growth were prepared from an elastomer, polydimethylsiloxane (PDMS; Sylgard 184, Dow Corning, Midland, MI), at 1:10 curing agent-to-monomer ratio and baked for 2 h at 60°C. The polymer was molded using metal templates. Surface microtopography was designed by acoustic micromachining, a technique developed in our laboratory (15). Cells were grown on flat (F) PDMS substrates as controls or on microgrooved (G) scaffolds. The surface topography included deep (50 μm deep, 120 μm wide) trapezoidal grooves separated by triangular ridges (Fig.
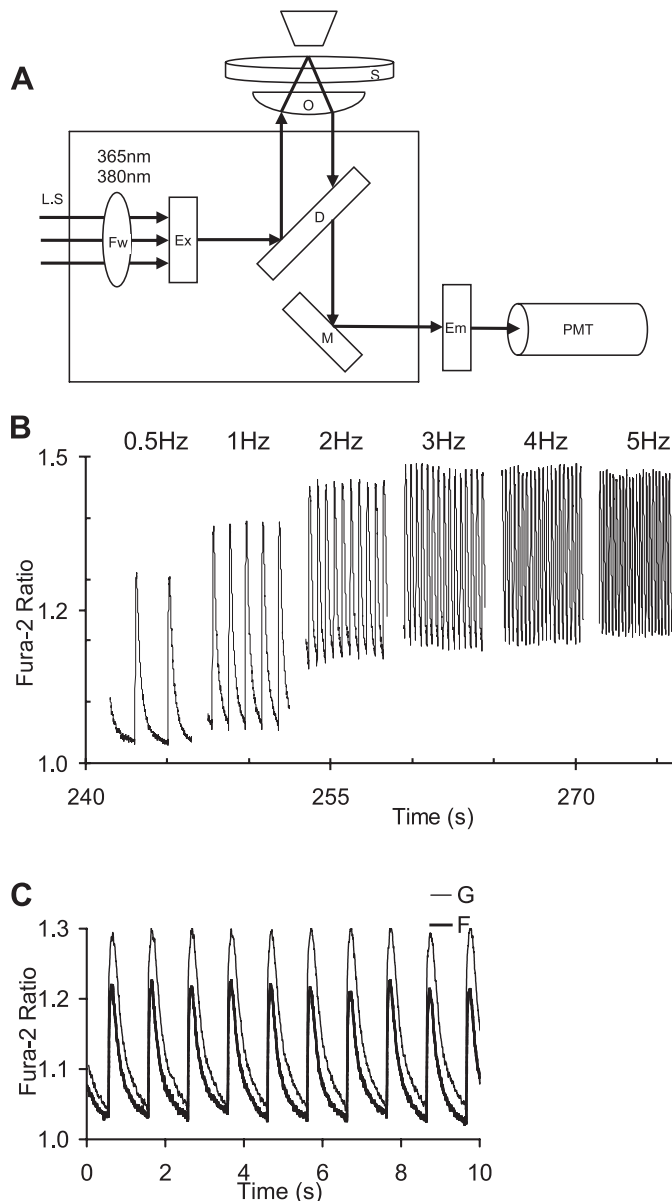

Fig. 2. Ca^{2+} transients measured as excitation ratio of fluorescence. *A*: schematic drawing of microscopic fluorescence system. Measurement system is built around an inverted microscope and includes light source (LS), filter wheel (Fw), excitation (Ex) filters (365 and 380 nm), cell sample (S), objective (O), dichroic mirror (D), reflective mirror (M), emission (Em) filter (510 nm), and photomultiplier tube (PMT). Excitation wavelengths are 365 nm (isobestic point) and 380 nm, and fluorescence intensities are determined through a 510-nm band-pass filter using a PMT. *B*: representative Ca^{2+} transients from a microgrooved sample at different pacing rates; 5 s of data are shown per frequency, which was changed from 0.5 to 5 Hz, maintaining stimulation for ≥30 s per frequency. *C*: comparison of intracellular Ca^{2+} concentration response to 1-Hz pacing in grooved (G) and flat (F) samples.

Table 1. *Ca^{2+} frequency dependence: fitting basic parameters*

Rank Sum Test	Sample Type	Curve Type	R	P			P for Each Pacing Frequency					
				k_1	k_2	k_3	0.5 Hz	1 Hz	2 Hz	3 Hz	4 Hz	5 Hz
Diastolic levels	G	$y = k_2 \cdot \ln(x) + k_1$	0.95±0.07	0.34	0.03*		0.13	0.34	0.22	0.16	0.15	0.09
	F		0.91±0.11									
Systolic levels	G	$y = k_1 \cdot (e^{-x/k_2} - e^{-x/k_3})$	0.99±0.01	0.02*	0.22	0.39	0.02*	0.01*	0.01*	0.02*	0.03*	0.05*
	F		0.98±0.02									
Width at 50%	G	$y = k_1 \cdot e^{-k_2 \cdot x}$	0.99±0.02	0.07	0.01*		0.12	0.13	0.27	0.34	0.06	0.02*
	F		0.99±0.01									

Values for correlation coefficient (*R*) are means ± SD. *Difference between flat (F) and grooved (G) samples at $P < 0.05$ by Wilcoxon's rank sum test.

1). To reveal structural organization, cardiomyocytes grown on microgrooves were stained using phalloidin-Alexa 488 (Molecular Probes, Eugene, OR) for F-actin and imaged using a confocal laser-scanning microscope (Radiance 2000, Bio-Rad) with a ×60 oil-immersion objective (NA 1.4), as described previously (6, 15).

Intracellular Ca^{2+} measurements. Ca^{2+} measurements were performed 4–6 days after culture in an experimental chamber perfused with oxygenated Tyrode solution (in mM: 1.33 CaCl$_2$, 5 glucose, 5 HEPES, 1 MgCl$_2$, 5.4 KCl, 135 NaCl, and 0.33 NaH$_2$PO$_4$, with pH adjusted to 7.4 using NaOH) at 30 ± 1°C. The pacemaking activity in G samples, confirmed under a microscope when the samples were removed from the incubator, was abolished in most cases after the culture medium was exchanged with Tyrode solution, the temperature was lowered, and fluorescent labeling was applied. This allowed external stimulation testing in such quiescent samples, as described below. Ca^{2+} transients in cells with persisting pacemaking under these conditions were measured but excluded from the restitution data. [Ca^{2+}]$_i$ levels were determined using a ratiometric fluorescence measurement technique (6). Cells were stained with the Ca^{2+}-sensitive dye fura 2 (8 μM; Molecular Probes) at room temperature for 20 min, and unincorporated stain was washed out for another 20 min. Electrical field stimulation (5–10 V/cm) was applied through built-in platinum electrodes in the side walls of the chamber using 5-ms biphasic pulses. Samples were imaged using an inverted fluorescence microscope (Nikon ×20 Fluor objective, NA 0.75) with excitation at 365 nm (isobestic point for fura 2) and 380 nm, and the fluorescence intensities were determined through a 510-nm band-pass filter using a photomultiplier detector (IonOptix, Milton, MA). The imaged area was restricted by a mechanical aperture to ∼200 × 100 μm in the central portion of the scaffold. The ratio of emission fluorescence intensities was calculated by taking the signal at 365 nm as numerator and the signal at 380 nm as denominator (Fig. 2A). External stimulation was applied at 0.5–5 Hz for ≥30 s per frequency (Fig. 2, B and C).

A two-point fura 2 calibration was performed at the end of some of the regular recordings according to the method of Grynkiewicz et al. (22) at zero and maximum Ca^{2+} levels. To obtain fluorescence ratios at saturating Ca^{2+} levels, 30 μM ionomycin (Molecular Probes) was applied to equilibrate intra- and extracellular Ca^{2+} concentration, the latter being increased to 13 mM. To measure fluorescence ratios at

zero intracellular Ca^{2+}, cells were treated with 10 mM EGTA (Molecular Probes), a Ca^{2+} chelator. The fluorescence ratio corresponding to maximum intracellular Ca^{2+} was recorded after 3 min of incubation with ionomycin at room temperature. Then ionomycin was replaced with the EGTA solution, and the fluorescence ratio under zero Ca^{2+} was measured in a similar way. Background fluorescence levels were recorded by imaging cell-free regions on the scaffolds.

To assess Ca^{2+} loading of the sarcoplasmic reticulum (SR), 30 mM caffeine (Sigma) was applied during quiescence after conditioning pacing at 0.5 Hz at room temperature. The caffeine-induced Ca^{2+} release in our cell networks was quantified by the area under the curve. Complete release was confirmed by lack of response thereafter and slow recovery of the transients on washout.

For a few cases, when transmembrane voltage was of interest, the cells were stained with the voltage-sensitive dye di-8-ANEPPS (50 μM; Molecular Probes) for 5 min. An appropriate set of filters (illumination at 535/50 nm, emission collection at 610/30 nm) was used with the same photodetector.

Optical testing of scaffolds. Even though a ratiometric technique resistant to environmental factors was used for Ca^{2+} measurements, we tested for possible optical effects of the surface texture on the recorded fluorescence signals. Several tests (with blind selection of the test spots) were performed on cell-free scaffolds having varied groove width. Scaffolds with groove spacing of 0 (flat) to 500 μm were prepared and illuminated at the same wavelengths used in the Ca^{2+} measurements. The fluorescence ratio for each sample was recorded for 5 min with the photomultiplier detector. The values at steady state were used for statistical analysis. To further probe for spatially varying optical effects from topographic features at the macroscopic scale, an intensified charge coupled device camera (Dage-MTI, Michigan City, IN) was used at constant gain to image 8 × 8 mm combined PDMS scaffolds (half flat and half grooved) submerged in a thin layer of water-soluble fura 2-pentapotassium salt (Molecular Probes) at high (1.33 mM Ca^{2+}) and zero Ca^{2+} levels (10 mM EGTA). Elimination of uneven illumination was accomplished through background subtraction of each wavelength before the addition of dye. Student's *t*-test was then performed with MATLAB (Mathworks, Novi, MI) to compare F and G regions.

Data processing and analysis. The raw experimental data, sampled at 1 kHz, were filtered using a Savitzky-Golay filter (width 9, order 2),

Table 2. *Ca^{2+} frequency dependence: fitting force-related parameters*

Rank Sum Test	Sample Type	Curve Type	R	P		P for Each Pacing Frequency					
				k_1	k_2	0.5 Hz	1 Hz	2 Hz	3 Hz	4 Hz	5 Hz
Total area	G	$y = k_1 \cdot e^{-k_2 \cdot x}$	0.99±0.01	<0.01*	0.16	<0.01*	<0.01*	<0.01*	<0.01*	0.09	0.16
	F		0.92±0.08								
Return velocity	G	$y = k_1 + k_2 x$	0.91±0.16	0.2	0.16	0.13	0.12	0.08	0.05*	0.06	0.05*
	F		0.95±0.02								
Relaxation time	G	$y = k_1 + k_2 x$	0.95±0.08	0.04*	0.02*	0.05*	0.07	0.16	0.31	0.02*	<0.01*
	F		0.93±0.07								

Values for *R* are means ± SD. *Difference between F and G samples at $P < 0.05$ by Wilcoxon's rank sum test.

and relevant parameters of the Ca^{2+} transients were automatically determined (IonWizard, IonOptix), including baseline, peak height, time to 50% peak, time to 50% baseline, peak time, maximum return velocity, and area under Ca^{2+} transients. Parameters for 10 Ca^{2+} transients per sample per frequency were used to fit empirical models for systolic Ca^{2+} level [$y = k_1(e^{-x/k_2} - e^{-x/k_3})$], diastolic Ca^{2+} levels [$y = k_2\ln(x) + k_1$], half-width ($y = k_1e^{-k_2x}$), total area under the Ca^{2+} transient ($y = k_1e^{-k_2x}$), maximum return velocity ($y = k_1 + k_2 \cdot x$), and relaxation time ($y = k_1 + k_2 \cdot x$) as a function of frequency using Microcal Origin 6.0 (OriginLab, Northampton, MA) or Microsoft Excel XP (Microsoft, Redmond, WA). The particular mathematical description of these relations was empirically determined so that the fit is reasonably good for each sample [correlation coefficient >0.9]. Each data set was fit by an individual curve across the examined frequencies to preserve inherent trends, and then the respective model parameters across samples were averaged to obtain representative curves. Because of the relatively small number of samples, statistical analysis (comparison between groups) was done using a nonparametric statistical test, i.e., Wilcoxon's rank sum test, in SigmaStat (Chicago, IL); P values were calculated using data after model fitting (Tables 1 and 2). The same statistics was applied to analyze the results of caffeine treatment.

RESULTS

Effects of topography on Ca^{2+} measurements. For unambiguous interpretation of the functional Ca^{2+} data, we first probed for possible interference of the surface texture with the fluorescence measurements. Optical testing of surfaces with variable groove spacing yielded no effects of topography on the [Ca^{2+}]$_i$ measurements ($P > 0.4$; Fig. 3A). Intensity ratios obtained from cell-free scaffolds with varied width spacing (2

per each type) were scattered in a small range of ratios (0.9–0.95; Fig. 3A). Autofluorescence from cells was also not a factor, inasmuch as fura 2-stained cardiomyocytes on G or F scaffolds at zero Ca^{2+} levels for calibration purposes (Fig. 3B) exhibited no significant difference.

Finally, no regional differences were found between F and G surfaces when imaged macroscopically with a charge coupled device camera (Fig. 3C). In the absence of any dye or cells, combination scaffolds (half flat, half grooved) had identical ratios. Use of water-soluble fura 2 to simulate high and low Ca^{2+} levels demonstrated no significant difference in intensity ratios. Therefore, we concluded that no optical artifact was introduced by the scaffold surface features or the cell's autofluorescence levels in our ratiometric measurements, allowing us to attribute measured differences to functional cellular behavior.

Fura 2 calibration. The diastolic and systolic [Ca^{2+}]$_i$ levels, obtained after calibration, were 30–50 and 85–190 nM, respectively, which fall at the low end of previously reported [Ca^{2+}]$_i$ values (34) but are consistent with data reported by Olbrich et al. (31). Difficulty in equilibrating intra- and extracellular Ca^{2+} concentration by ionomycin, mainly due to dye uptake and compartmentalization in mitochondria and SR, incomplete dye hydrolysis, or cell hypercontracture, might have contributed to the comparatively low values. Various calibration approaches have been attempted to address the above-mentioned problems, including ion equilibration, metabolism inhibition (18), or butanedione monoxime treatment (9). However, none of these approaches can resolve all the limitations simultaneously. Be-
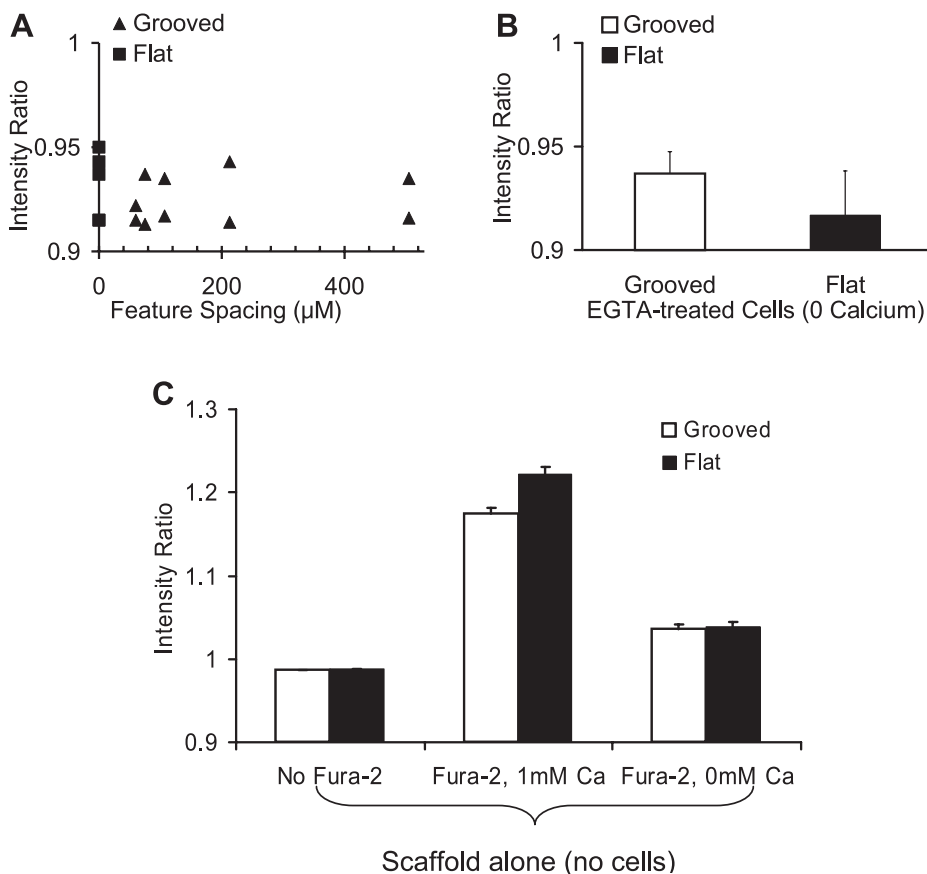
Fig. 3. Scaffold geometry does not affect optical measurements. *A*: ratio recordings on empty G scaffolds (without cells or dye) and varied feature spacing (ridge-to-ridge spacing) demonstrated no obvious trend or difference from F scaffolds ($P > 0.4$). *B*: fura 2-stained cardiomyocytes on G and F scaffolds at zero Ca^{2+} employed for calibration purposes ("Ca^{2+}-free cells") also exhibited no significant difference ($P > 0.05$): 0.94 ± 0.01 ($n = 19$) and 0.92 ± 0.02 ($n = 8$) for G and F, respectively. *C*: macroscopic charge-coupled device imaging of combined F and G polydimethylsiloxane scaffolds demonstrated no difference in fluorescence intensity ratios when placed in Tyrode solution (no fura 2: 0.99 ± 0.001 and 0.99 ± 0.001 for G and F, respectively) or fura 2 (K$^+$ salt) calibration solution at 1.33 mM Ca^{2+} (1.17 ± 0.007 and 1.22 ± 0.008 for G and F, respectively) and 0 mM Ca^{2+} (1.04 ± 0.006 and 1.04 ± 0.006 for G and F, respectively). Values are means $\pm$ SE.
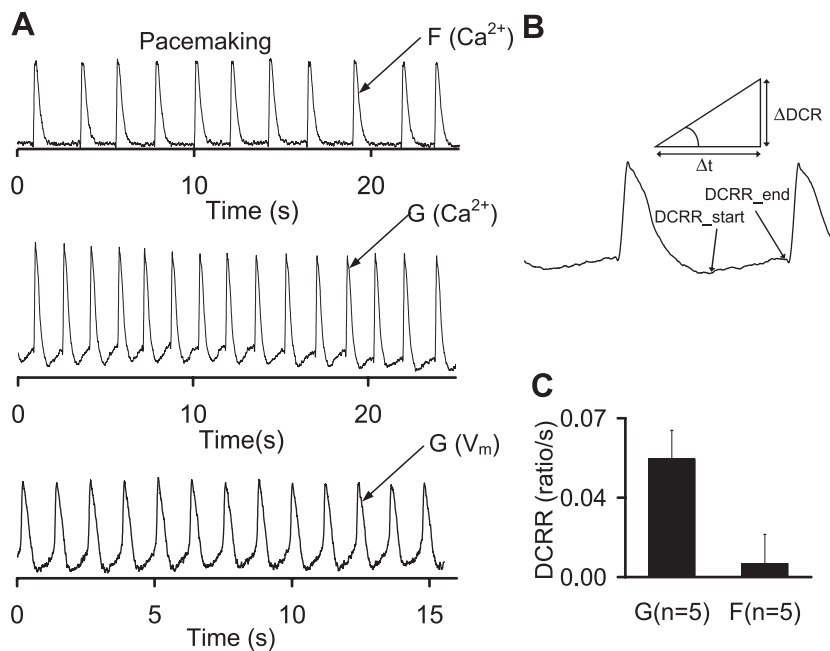
Fig. 4. Pacemaking in G samples. *A*: synchronous pacemaking was more commonly observed in G than in F samples. Spontaneous Ca^{2+} transients in G samples exhibited more pronounced slow diastolic Ca^{2+} rise (DCR). Slow depolarization was also found in the voltage (V_m) signal on G scaffolds (*bottom trace*), as measured using a voltage-sensitive dye. *B*: DCR rate (DCRR) was determined as DCRR = ($\Delta DCR/\Delta t$) in nonpaced traces after automatic detection of DCRR start (time of lowest ratio level during diastole) and DCRR end (starting time of Ca^{2+} upstroke). *C*: G samples exhibited significantly higher DCRR than F samples (0.05 ± 0.01 vs. 0.006 ± 0.01, $n = 5$ each, $P < 0.02$). Among F samples, 4 showed negative DCRR and 1 had positive DCRR. Values are means $\pm$ SE.

cause of the difficulties associated with fura 2 calibration, instead of actual Ca^{2+} concentration, we chose to present our data in intensity ratios. Furthermore, we are interested in relative differences between microgrooved samples and controls; therefore, the absolute values of $[Ca^{2+}]_i$ were not essential in our case.

Pacemaking in microgrooved samples. The first striking functional difference between F and G samples was higher incidence of synchronized spontaneous activity in cardiac networks on topographically modified than on flat surfaces, as reported previously (6, 15). In this study, we analyzed $[Ca^{2+}]_i$ transients during this pacemaking activity in F and G scaffolds and found significantly higher diastolic Ca^{2+} rise rate (DCRR,

Fig. 4*B*) on nonpaced G samples than on F samples (means $\pm$ SE: 0.05 ± 0.01 and 0.006 ± 0.01 for G and F, respectively, $n = 5$ each, $P < 0.02$; Fig. 4*C*). High DCRR (7–40 nM/s) has been linked to ectopic activity (2). Our calibration-converted DCRR values (Fig. 4*C*) fall in a similar range (20–50 nM/s), suggesting a possible Ca^{2+} involvement in the observed pacemaking behavior on microgrooved surfaces. The occurrence of diastolic Ca^{2+} rise was matched by slow diastolic depolarization in optically obtained voltage traces (membrane potential) from G samples (Fig. 4*A*).

Alterations in basic $[Ca^{2+}]_i$ frequency dependence. To determine whether surface topography brings about changes in intracellular Ca^{2+} dynamics and to quantify the extent of these
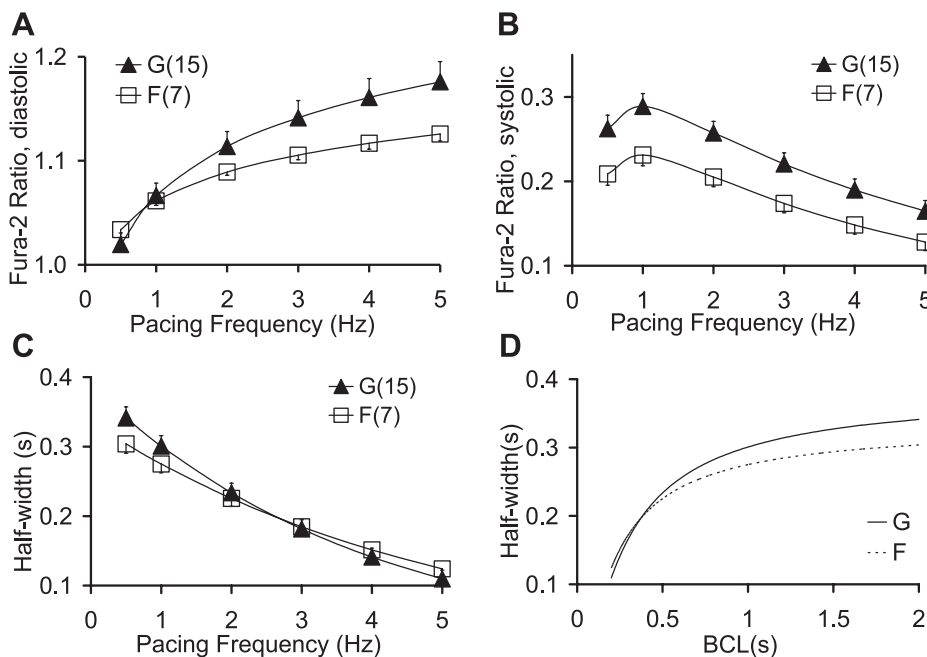

Fig. 5. Topography-influenced Ca^{2+} frequency dependence of basic parameters. *A*: frequency sensitivity of diastolic levels was higher for G than for F samples. *B*: G and F samples followed a biphasic dependence of peak systolic levels on frequency. G transients had higher peak systolic levels over the entire frequency range. *C*: G samples had steeper decrease in half-width with frequency than F samples. *D*: in an alternative representation of *C* using basic cycle length (BCL), G samples demonstrated a steeper restitution curve.

changes, we characterized Ca^{2+} transients under external electrical stimulation in the frequency range 0.5–5 Hz. Higher diastolic $[Ca^{2+}]_i$ levels were induced in G than in F samples by high-frequency pacing. The curve relating diastolic Ca^{2+} to frequency was steeper for G than for F samples [reflected in the slope k_2 in the fitted equation (Table 1); mean $\pm$ SE: 0.07 ± 0.007 for G ($n = 15$ scaffolds) and 0.04 ± 0.006 for F ($n = 7$ scaffolds), $P < 0.05$; Fig. 5A]. The curves for the two cases started from identical low-frequency levels but diverged at higher frequencies.

The frequency response of systolic $[Ca^{2+}]_i$, assessed as the peak ratio value minus the diastolic level, was empirically found to follow a nonmonotonic curve, which was modeled as a sum of two exponents. About 80% of the G samples and 86% of the F samples followed the biphasic curve, peaking at 1 Hz, which indicates a combination of positive and negative Ca^{2+}-frequency relations in both cases. The rest of the samples had a monotonic decline, i.e., a negative Ca^{2+}-frequency relation. Peak systolic levels of Ca^{2+} transients were consistently higher at all frequencies in G than in F samples, as found in significantly different amplitudes (k_1) of the fitted biexponential curves [mean $\pm$ SE: 0.31 ± 0.02 for G ($n = 7$) and 0.25 ± 0.01 for F ($n = 15$), $P < 0.05$] and also in different individual frequency-dependent Ca^{2+} systolic levels, except at 5 Hz (Table 1, Fig. 5B).

The half-width of the Ca^{2+} transients, defined as the interval between time to 50% peak and time to 50% baseline, experienced different dynamics across the frequency range for F and G samples. For both cases, a single decay exponential function was found to represent well the frequency dependence of this parameter, related to the Ca^{2+} restitution characteristics. Significant differences between F and G samples were observed in the time constant (k_2) of the fitted curves [mean $\pm$ SE: $k_2 = 0.25 \pm 0.01$ for G ($n = 15$) and 0.2 ± 0.02 for F ($n = 7$), $P < 0.01$; Table 1, Fig. 5C]. An alternative representation of the data using basic cycle length, more typical for analysis of restitution, is also shown (Fig. 5D). Along with the statistically significant difference in the slope ($P < 0.01$) between F and G samples, a trend for longer-lasting transients for the G samples at low frequencies was also noted.

Alterations in estimated force parameters. If $[Ca^{2+}]_i$ and force are linked in the same way for F and G samples, i.e., if similar Ca^{2+} sensitivity is observed, then the total area under the Ca^{2+} transients, reflecting total available Ca^{2+} for contraction, can be used as an estimator of force. Data from both groups fit well monoexponential decay curves, possibly indicating a negative force-frequency relation. Cardiac networks on G scaffolds had higher overall areas than those on F surfaces, hinting at higher tension developed [significant increase in amplitude k_1 of the fitted curve (Table 2); mean $\pm$ SE: 0.13 ± 0.01 for G ($n = 15$) and 0.08 ± 0.01 for F ($n = 7$), $P < 0.01$]. A convergence of the F and G curves to a common value was noted at higher pacing frequencies.

Maximum return velocity and relaxation time, defined as time to 50% baseline minus peak time, reflect important aspects of cell relaxation kinetics. Frequency responses of both parameters followed a monotonic linear relation (Fig. 6, B and C, Table 2), consistent with frequency-dependent acceleration of relaxation. Table 2 presents data pointing to overall faster (but nonsignificant) return velocities of G than of F surfaces over the examined frequency range. Furthermore, relaxation
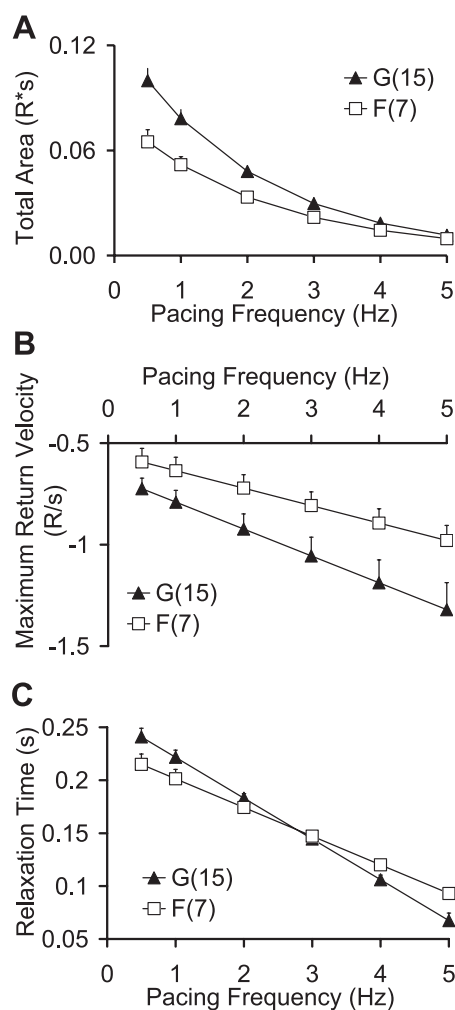

Fig. 6. Topography-influenced Ca^{2+} frequency dependence of parameters related to estimated force development. *A*: total area under Ca^{2+} transients at all frequencies was larger in G than in F samples. R*s, ratio $\times$ sec. *B*: frequency-dependent increase in maximum return velocity was stronger in G than in F samples. R/s, ratio/sec. *C*: frequency-dependent decrease in relaxation time was stronger in G than in F samples.

time of G samples adapted faster to increased pacing rates [higher slope (k_2), $P < 0.02$]. This behavior paralleled the steeper restitution of the half-width (Fig. 5, *C* and *D*) and suggests that dynamic adaptation of the Ca^{2+} transients is predominantly driven by changes in the relaxation phase.

Instabilities in Ca^{2+} dynamics in microgrooved samples. Spontaneous Ca^{2+} release of variable magnitude was observed in G samples after fast pacing (Fig. 7A), in agreement with the elevated diastolic $[Ca^{2+}]_i$ on grooved surfaces at higher frequencies (Fig. 5A). Dynamic instabilities in Ca^{2+}, known as Ca^{2+} alternans, were much more likely to occur in G samples under higher pacing rates than in their F counterparts at the same frequency (Fig. 7B). Alternans occurrence in G samples was more than three times higher than in F samples [39% in G ($n = 33$) and 12.5% in F ($n = 16$)]. The Ca^{2+} alternans were paralleled by voltage alternans (Fig. 7B), the occurrence of which is known to be facilitated by a steeper restitution response (19).

SR load assessed by caffeine-induced Ca^{2+} release. To test whether higher frequency of spontaneous Ca^{2+} release is a
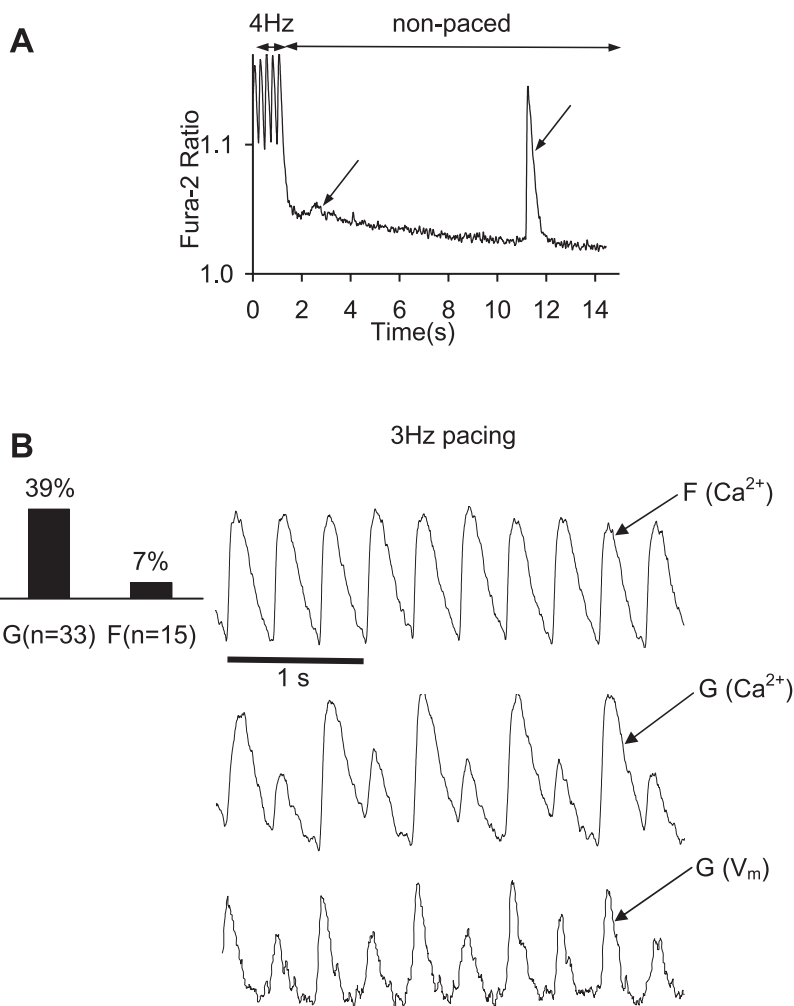
A

Fig. 7. Electromechanical instabilities in G samples. *A*: after rapid pacing at 4 Hz, G samples were more prone to generate spontaneous Ca^{2+} release (arrows). A similar phenomenon was observed in only 1 F sample. *B*: at the same pacing frequency (3 Hz), G samples were more likely than F samples to exhibit Ca^{2+} and voltage alternans. *Inset*: statistics on occurrences of Ca^{2+} alternans in F and G samples.

B

consequence of an elevated SR load, we conducted an indirect assessment by quantification of caffeine-induced Ca^{2+} release. A statistical difference ($P < 0.02$ by nonparametric test) in the area under the curve of the release was observed for G samples ($n = 9$) vs. F samples ($n = 9$), suggesting an increased SR load in the G samples (Fig. 8). Interpreting caffeine-induced Ca^{2+} release in a multicellular preparation is not a trivial task because of possible propagation into the imaged region. However, both groups were subjected to identical conditions, with all release events taken into account. A complete depletion of the SR was confirmed by resuming pacing and then observing recovery on reperfusion with caffeine-free Tyrode solution. Quantification of additional related parameters revealed statistically higher peak release ($P < 0.03$), higher duration of the overall release ($P < 0.04$), and higher number of pulses ($P < 0.03$) for G than for F samples.

DISCUSSION

Despite the prominent role of Ca^{2+} as a ubiquitous second messenger, mediator of force development, and modulator of arrhythmia, little is known about direct effects of tissue structure on intracellular Ca^{2+} dynamics. Using a cultured cardiomyocyte model, we sought to determine whether simple topographic features, enforcing cell rearrangement, influence functional Ca^{2+} handling and whether the altered Ca^{2+} behavior

results in a proarrhythmic state. As used here, cultured cardiomyocyte networks provide a model for probing structure-function relations by permitting fine control of cellular structure through manipulation of three-dimensional scaffold architecture. Basic cellular responses characterized in this versatile model build a foundation for further studies, especially when a well-defined system is required, e.g., screening for drug toxicity or efficacy (29), as well as efforts in cardiac tissue engineering (1).

Topography-altered Ca^{2+} handling. Our results for the control (F) and G samples (Fig. 5*A*) confirm elevation in diastolic [Ca^{2+}] with higher pacing rates, a well-documented physiological response (7, 11). Although both groups start at identical resting Ca^{2+} levels at low frequencies, the G samples tend to accumulate Ca^{2+} faster at increased pacing rates. Underlying this process can be altered Ca^{2+} fluxes in the G vs. F case, which ultimately can crucially contribute to the observed pacemaking activity by facilitating spontaneous Ca^{2+} release.

Peak systolic Ca^{2+}-frequency data in this study indicate a biphasic relation for F and G samples, with G being offset to higher peak systolic Ca^{2+} levels throughout the frequency range (Fig. 5*B*). Even though no direct force measurements were performed, an integral Ca^{2+} availability measure (area under the Ca^{2+} transient) was used to assess force. In this representation, a monotonic declining relation emerged for F
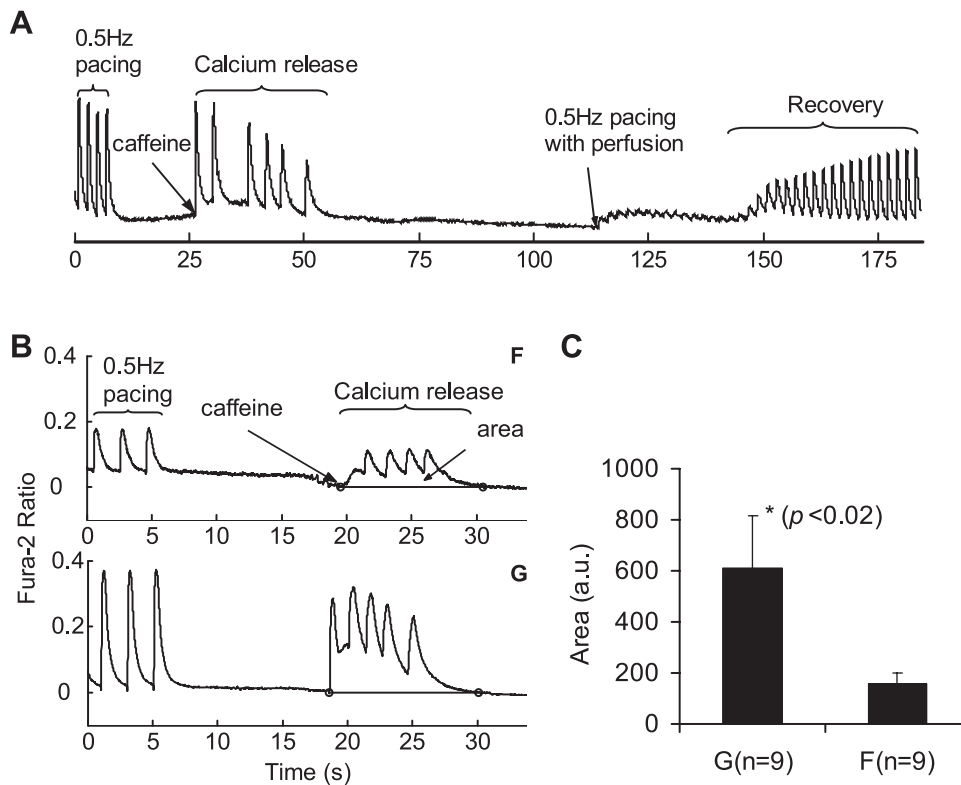
Fig. 8. Sarcoplasmic reticulum load assessment via caffeine-triggered release. *A*: protocol for experiments showing 0.5-Hz preconditioning, caffeine-induced Ca^{2+} release, and subsequent recovery on perfusion with caffeine-free solution. *B*: traces from F (*top*) and G (*bottom*) samples, with illustration of the area calculations. *C*: summary of results, with area in arbitrary units (au). Values are means $\pm$ SE; $n = 9$ cultures per group.

and G (Fig. 6*A*), likely a result of faster adaptation of Ca^{2+} transient duration (Fig. 5*C*) interacting with the biphasic peak systolic trend (Fig. 5*B*). This overall negative force-frequency relation is usually attributed to relatively high SR loading, even at low pacing rates (5). Force estimates were greater for G than for F samples but converged to identical values at high frequencies. These results are consistent with our previous findings for increased tension and higher cellular strains in the G samples (6, 15). Placing these results in context, we note that previous studies have reported negative (4, 24), positive, and biphasic (26) force-frequency relations for the rat. Although, in most mammalian hearts, increasing frequency of stimulation results in greater forces developed, the rat cardiac muscle's frequency response remains controversial. Often the negative force-frequency relation, uniquely observed in rat preparations, has been considered an artifact and attributed to inadequate perfusion (thick specimens). The multicellular experimental system used in this study, having a thickness below the 100-μm perfusion limit, is unlikely to suffer from such limitations, thereby providing an interesting test bed for this basic question.

Extending our Ca^{2+}-handling characterization to parameters related to the kinetics of the frequency response, we observed steeper curves (higher sensitivity to frequencies) for G than for F samples in several instances: half-width (Fig. 5*C*), maximum return velocity (Fig. 6*B*), and relaxation time (Fig. 6*C*). Frequency-dependent acceleration of relaxation (FDAR) in force measurements has been reported as a universal property of the cardiac muscle (13), helping the diastolic filling of the heart, and is often paralleled by a similar Ca^{2+}-related relaxation phenomenon. Our in vitro model, in its monolayer version (F) and its topographically modified version (G), exhibits a strong

FDAR trend (Fig. 6, *B* and *C*). The data reported here indicate dominant adaptation of the relaxation phase of the Ca^{2+} transients to pacing rates compared with the changes in the upstroke phase. This links directly Ca^{2+} restitution (width-frequency) to FDAR (relaxation time-frequency), which might carry important implications for the electromechanics of these cells at high pacing rates.

Pacemaking, Ca^{2+} frequency dependence, and arrhythmogenesis. Aberrations in intracellular Ca^{2+} handling (increased diastolic Ca^{2+}) have been embraced as possible pathways to arrhythmogenesis by nonreentrant ectopic activity, such as triggered arrhythmias (3). We corroborate such a relation in our model on the basis of observations of spontaneous Ca^{2+} release after high pacing rates (Fig. 7*A*) and increased diastolic Ca^{2+} rise rates (Fig. 4), leading to a pacemaking type of behavior in the G samples. Although pacemaking has been traditionally linked to the hyperpolarization-activated current (I_f), recent evidence points to multiple molecular mechanisms, often centered around spontaneous release from the SR (27). Indirect assessment of the SR load by caffeine-induced Ca^{2+} release revealed a significantly higher load for G than for F samples (Fig. 8). This might explain accumulation of Ca^{2+} at high pacing rates in G samples. This method does not differentiate between alterations in the mechanisms controlling the influx and the outflux of Ca^{2+} from the SR. Whether in our case pacemaking was purely Ca^{2+} driven or additional changes in ion currents took place after the cell rearrangement is yet to be explored. The implications of this finding are that cell phenotype might be controllable to a certain extent via the provided microenvironment. In a pathological setting, changes in Ca^{2+} handling after structural heart disease, with extensive fibrosis (mimicked in our model system by extreme cellular

anisotropy and reduced transgroove connectivity), could be an important contributing factor to readily observed triggered arrhythmias by Ca^{2+}-related pathways (32).

Furthermore, there has been recent interest in Ca^{2+} dynamics as a contributing factor in the development of electromechanical instabilities, known as alternans, important in reentrant arrhythmias. The action potential duration (APD) restitution hypothesis offers an explanation for the deterioration of a stable reentrant activation into a fibrillatory pattern (19, 21). Under this hypothesis, electrical instabilities (alternans) occur as a direct result of a steeper APD-frequency response and form the prelude to fibrillation. Whether steepness of the Ca^{2+} restitution can serve a similar predictive role for proarrhythmic behavior is not known, but the key role of the L-type Ca^{2+} channel (main entry/trigger in Ca^{2+} handling) in APD restitution and in the onset of alternans has been established (21). Our findings convincingly point to a greater incidence of Ca^{2+} alternans in the G samples (Fig. 7B), which also had steeper (Ca^{2+}) restitution. This association, however, needs to be probed further for a direct cause-effect relation.

Limitations. Evidence that topography-mediated aberrations in Ca^{2+} handling increase susceptibility to arrhythmias is presented along with transmembrane voltage dynamic instabilities, but whether Ca^{2+} changes are the cause of voltage alternans or reflective of transmembrane potential irregularities remains to be determined. Simultaneous Ca^{2+} and membrane potential recordings are required for demonstration of a causal relation. Voltage and ion channel data are also needed to explore other electrophysiological differences between the two groups. In addition, we present single-channel data in the temporal domain lacking spatial information, which leaves topographic influences on cellular connectivity and conduction uncertain. Spatial mapping of Ca^{2+} and electrical activity can reveal anisotropic conduction and better elucidate mechanisms of initiation and maintenance of arrhythmias. Particularly interesting is whether reduced gap junction connectivity at intergroove borders and increased anisotropy provide a mechanism by which ectopic sites can more easily escape, causing functional reprogramming toward a proarrhythmogenic state as a direct result of topography.

In conclusion, we present the first data on frequency-dependent Ca^{2+} handling in a cultured cardiomyocyte model system that are suitable for mechanistic studies of a structure-function relation and, at the same time, serve as a model system in basic research toward cardiac tissue engineering for heart replacement. Our findings show that a simple geometric modification in the cellular microenvironment (scaffold topography) can result in substantial functional remodeling and eventually lead to some proarrhythmic changes via Ca^{2+}-dependent pathways involving increased SR loading.

REFERENCES

1. **Akins RE.** Can tissue engineering mend broken hearts? *Circ Res* 90: 120–122, 2002.
2. **Arutunyan A, Swift LM, and Sarvazyan N.** Initiation and propagation of ectopic waves: insights from an in vitro model of ischemia-reperfusion injury. *Am J Physiol Heart Circ Physiol* 283: H741–H749, 2002.
3. **Baartscheer A, Schumacher CA, Belterman CN, Coronel R, and Fiolet JW.** SR calcium handling and calcium after-transients in a rabbit model of heart failure. *Cardiovasc Res* 58: 99–108, 2003.
4. **Bers DM.** SR Ca loading in cardiac muscle preparations based on rapid-cooling contractures. *Am J Physiol Cell Physiol* 256: C109–C120, 1989.
5. **Bers DM.** *Excitation-Contraction Coupling and Cardiac Contractile Force.* Dordrecht: Kluwer Academic, 1993.
6. **Bien H, Yin L, and Entcheva E.** Cardiac cell networks on elastic microgrooved scaffolds. *IEEE Eng Med Biol Mag* 22: 108–112, 2003.
7. **Brixius K, Pietsch M, and Schwinger RH.** The intracellular Ca^{2+} homeostasis influences the frequency-dependent force-generation in man. *Basic Res Cardiol* 94: 152–158, 1999.
8. **Bursac N, Parker KK, Iravanian S, and Tung L.** Cardiomyocyte cultures with controlled macroscopic anisotropy: a model for functional electrophysiological studies of cardiac muscle. *Circ Res* 91: E45–E54, 2002.
9. **Cheung JY, Tillotson DL, Yelamarty RV, and Scaduto RC Jr.** Cytosolic free calcium concentration in individual cardiac myocytes in primary culture. *Am J Physiol Cell Physiol* 256: C1120–C1130, 1989.
10. **Chou L, Firth JD, Uitto VJ, and Brunette DM.** Effects of titanium substratum and grooved surface topography on metalloproteinase-2 expression in human fibroblasts. *J Biomed Mater Res* 39: 437–445, 1998.
11. **Clusin WT.** Calcium and cardiac arrhythmias: DADs, EADs, and alternans. *Crit Rev Clin Lab Sci* 40: 337–375, 2003.
12. **Curtis A and Wilkinson C.** Topographical control of cells. *Biomaterials* 18: 1573–1583, 1997.
13. **DeSantiago J, Maier LS, and Bers DM.** Frequency-dependent acceleration of relaxation in the heart depends on CaMKII, but not phospholamban. *J Mol Cell Cardiol* 34: 975–984, 2002.
14. **Deutsch J, Motlagh D, Russell B, and Desai TA.** Fabrication of microtextured membranes for cardiac myocyte attachment and orientation. *J Biomed Mater Res* 53: 267–275, 2000.
15. **Entcheva E and Bien H.** Tension development and nuclear eccentricity in topographically controlled cardiac syncytium. *J Biomed Microdev* 5: 163–168, 2003.
16. **Entcheva E, Yin L, and Bien H.** $[Ca^{2+}]_i$ changes in cardiac tissue constructs on 3D elastic matrices (Abstract). *PACE Pacing Clin Electrophysiol* 26: 1107, 2003.
17. **Fast V and Kleber A.** Anisotropic conduction in monolayers of neonatal rat heart cells cultured on collagen substrate. *Circ Res* 75: 591–595, 1994.
18. **Frampton JE, Orchard CH, and Boyett MR.** Diastolic, systolic and sarcoplasmic reticulum $[Ca^{2+}]$ during inotropic interventions in isolated rat myocytes. *J Physiol* 437: 351–375, 1991.
19. **Garfinkel A, Kim YH, Voroshilovsky O, Qu Z, Kil JR, Lee MH, Karagueuzian HS, Weiss JN, and Chen PS.** Preventing ventricular fibrillation by flattening cardiac restitution. *Proc Natl Acad Sci USA* 97: 6061–6066, 2000.
20. **Geiger B.** Cell biology. Encounters in space. *Science* 294: 1661–1663, 2001.
21. **Gilmour RF Jr.** A novel approach to identifying antiarrhythmic drug targets. *Drug Discov Today* 8: 162–167, 2003.
22. **Grynkiewicz G, Poenie M, and Tsien RY.** A new generation of Ca^{2+} indicators with greatly improved fluorescence properties. *J Biol Chem* 260: 3440–3450, 1985.
23. **Hein S, Elsasser A, Kostin S, Zimmermann R, and Schaper J.** Functional disturbances due to structural remodeling in the failing human heart. *Arch Mal Coeur Vaiss* 95: 815–820, 2002.
24. **Hoffman BF and Kelly JJ.** Effects of rate and rhythm on contraction of rat papillary muscle. *Am J Physiol* 197: 1199–1204, 1959.
25. **Howarth FC, Boyett MR, and White E.** Rapid effects of cytochalasin-D on contraction and intracellular calcium in single rat ventricular myocytes. *Pflügers Arch* 436: 804–806, 1998.

26. **Layland J and Kentish JC.** Positive force- and [Ca^{2+}]-frequency relationships in rat ventricular trabeculae at physiological frequency. *Am J Physiol Heart Circ Physiol* 276: H9–H18, 1999.

27. **Lipsius SL, and Bers DM.** Cardiac pacemaking: I_F vs. Ca^{2+}, is it really that simple? *J Mol Cell Cardiol* 35: 891–893, 2003.

28. **McDevitt TC, Angello JC, Whitney ML, Reinecke H, Hauschka SD, Murry CE, and Stayton PS.** In vitro generation of differentiated cardiac myofibers on micropatterned laminin surfaces. *J Biomed Mater Res* 60: 472–479, 2002.

29. **Nave BT, Becker M, Roenicke V, and Henkel T.** Validation of targets and drug candidates in an engineered three-dimensional cardiac tissue model. *Drug Discov Today* 7: 419–425, 2002.

30. **Oakley C and Brunette DM.** Topographic compensation: guidance and directed locomotion of fibroblasts on grooved micromachined substrata in the absence of microtubules. *Cell Motil Cytoskeleton* 31: 45–58, 1995.

31. **Olbrich HG, Donck LV, Geerts H, Mutschler E, Kober G, and Kaltenbach M.** Cyclosporine increases the intracellular free calcium concentration in electrically paced isolated rat cardiomyocytes. *J Heart Lung Transplant* 12: 652–658, 1993.

32. **Pogwizd SM.** Nonreentrant mechanisms underlying spontaneous ventricular arrhythmias in a model of nonischemic heart failure in rabbits. *Circulation* 92: 1034–1048, 1995.

33. **Swynghedauw B.** Molecular mechanisms of myocardial remodeling. *Physiol Rev* 79: 215–262, 1999.

34. **Toraason M, Wey HE, Richards DE, Mathias PI, and Krieg E.** Altered Ca^{2+} mobilization during excitation-contraction in cultured cardiac myocytes exposed to antimony. *Toxicol Appl Pharmacol* 146: 104–115, 1997.

35. **Walsh KB and Parks GE.** Changes in cardiac myocyte morphology alter the properties of voltage-gated ion channels. *Cardiovasc Res* 55: 64–75, 2002.